J Mater Sci: Mater Electron (2021) 32:28792–28806

Electrical properties of Ga/V-modified ZnO ceramic thistors

Bicai Li[1,2], Zhicheng Li[1], Shuyan Zhang[1], Dicheng Peng[1], Caiyun Gao[1], and Hong Zhang[1,*]

[1] School of Materials Science and Engineering, Central South University, Changsha 410083, China
[2] School of Materials and Chemical Engineering, Hunan City University, Yiyang 413000, China

Received: 23 September 2021
Accepted: 17 October 2021
Published online: 27 October 2021

ABSTRACT

The $Zn_{1-x}Ga_xO$ (x = 0–0.020) ceramics modified with V_2O_5 were prepared by solid-state reaction method. The phase composition, microstructure, electrical conductivity, temperature sensitivity, and thermal aging property were investigated. The main phase of prepared ceramics is a hexagonal wurtzite crystal structure with a space group of $P6_3mc$ (186). Ga_2O_3 phase was detected in ceramics when the content of Ga-ion x is higher than 0.010. V_2O_5 acts as sintering aids and electrical stabilizer and enhanced the ceramic sintering ability. The Ga/V-modified ZnO ceramics exhibit typical NTC characteristics and have high temperature sensitivity with material constant of B values ranging from 3659 to 4590 K. The electrical properties and aging characteristics were studied with alternating current impedance spectrum and X-ray photoelectron spectroscopy. The Ga/V-co-modified ZnO ceramics show high electrical stability with resistance change rate ($\Delta R/R_0$) less than 1.85% after aged at 150 °C for 1000 h. The increase of resistance by aging mainly came from the grain boundary effect.

1 Introduction

A negative temperature coefficient (NTC) thermistor shows that its resistivity decreases with increase of temperature, especially, is characterized by that its resistivity decreases exponentially with the increase of temperature. NTC thermistors are widely applied in various fields, such as temperature compensation, temperature measurement and control, surge current suppression, and infrared detection. The researches of the ordinary temperature NTC ceramic thermistors are mainly based on spinel structure compounds [1–3], perovskite compounds [4–6], and semiconductors based on single cationic oxides [7–9]. The small polaron hopping model is generally considered to be the conduction mechanism of AB_2O_4-type spinel compounds, in which the charge carriers hop between octahedral B-sites such as Mn^{3+}–Mn^{4+} ions in manganate spinel compounds [1, 2, 10, 11]. Meanwhile, both the band conduction and electron-hopping models were suggested for the conduction mechanism of semiconductor-type NTC thermistors

Address correspondence to E-mail: hzhang@csu.edu.cn

https://doi.org/10.1007/s10854-021-07264-9

[12–14]. Based on the above multi-model conduction mechanisms, the room-temperature resistivity (ρ_{25}) and temperature sensitivity ($B_{25/85}$ value) of semiconductor-type thermistors could be effectively adjusted through appropriate ion doping. As reported by Wang et al. [13], ρ_{25} from 64.14 Ω·cm to 43.37 kΩ·cm and $B_{25/85}$ from 335 to 5169 K were obtained in Li/Fe-modified NiO NTC thermistors. Yang et al. reported that adjustable ρ_{25} (12.38 Ω·cm–190 kΩ·cm) and $B_{25/85}$ (1112–4376 K) in CuO-based NTC thermistors were prepared by changing the contents of Y_2O_3 and B_2O_3 [14].

Besides ρ_{25} and $B_{25/85}$ values, electrical stability is also an important property for a NTC thermistor. The electrical stability is normally characterized by resistance change rate ($\Delta R/R_0$) through aging treatment with various periods. The electrical stability of NTC thermistor can be improved by element doping and/or optimization of preparation process [7, 15, 16]. Li et al. showed that Na-ion doping reduced the resistivity and $\Delta R/R_0$ of $Mn_{1.95}Co_{0.21}Ni_{0.84}O_4$ ceramics [15]. Gao et al. found that the electrical stability of $(Zn_{0.4}Ni_{0.6})_{1-x}Na_xO$ NTC thermistors was greatly enhanced with the addition of Bi-ion and the $\Delta R/R_0$ was reduced from 237 (without Bi_2O_3) to 1.8% (with Bi_2O_3) [16]. Sb/Mn-co-doped SnO_2 ceramics showed high electrical stability, and the $\Delta R/R_0$ of $Sn_{0.91}Sb_{0.05}Mn_{0.04}O_2$ was only 0.6% after aging 500 h in air [7].

ZnO is a typical environmental friendly material with a low cost price, non-toxic, and harmless. Due to its wide band gap (− 3.37 eV), ZnO has been widely used in the fields of luminescence, photocatalysis, varistor, and piezoelectricity [17–20]. In recent years, the researches on ZnO-based thermistors have also been reported. Li/Y/Cr-co-doped ZnO ceramics showed a critical positive temperature coefficient (PTC) phenomenon with a resistivity temperature coefficient as high as 65% K^{-1} [21]. Li et al. reported that ZnO-based ceramics co-modified with Al-, La-, and Cu-ions showed good performance for NTC thermistors with controllable ρ_{25} (0.65–3280 kΩ·cm) and $B_{25/85}$ values (2500–5850 K) and high electrical stability ($\Delta R/R_0 < 2\%$) [22]. To further develop the application of ZnO-based ceramics for NTC thermistors, Ga-doped ZnO ceramics modified with V_2O_5 were investigated in this work. The ceramics exhibit typical NTC characteristics with high temperature sensitivity ($B_{25/85}$ value) and electrical stability.

2 Experimental

$Zn_{1-x}Ga_xO$ (x = 0, 0.002, 0.004, 0.006, 0.008, 0.010, 0.012, 0.014, 0.016, 0.018, and 0.020, respectively) ceramics were synthesized with conventional solid-state reaction method. Small amount of V_2O_5 (from 0.125 to 1.0% in mass ratio) was used as sintering aids and electrical stabilizer. Analytical reagent grade (purity > 99%) ZnO, Ga_2O_3, and V_2O_5 from the Sinopharm Chemical Reagent Co., Ltd, China were used as raw materials. According to the stoichiometric ratio of nominal formula $Zn_{1-x}Ga_xO$, the weighed ZnO and Ga_2O_3 powders were mixed by ball milling for 1 h and then were calcined at 900 °C for 5 h in air. For each batch, various contents of V_2O_5 were added into the calcined powder followed by grinding and mixing for 1 h. An appropriate amount of polyvinyl alcohol solution (PVA) solution (Sinopharm Chemical Reagent Co., Ltd, China) was used as binder during granulating. Then pellets with a diameter of 12 mm and a thickness of about 3 mm were obtained. The pellets were sintered at 1150 °C for 5 h followed by 1350 °C for 2 h in air. The surfaces of as-sintered pellets were ground with abrasive paper. Silver paste was painted on both opposite surfaces and then was heated at 600 °C for 10 min to make ohmic electrodes.

Phase composition of the as-sintered $Zn_{1-x}Ga_xO$ ceramics was identified by X-ray diffraction (XRD, Rigaku D/Max 2500, Japan) with Cu Kα radiation. Fracture surface of broken ceramics was examined by a scanning electron microscopy (SEM, JMS-7900F), and the related elemental distribution was analyzed with energy-dispersive X-ray spectroscopy (EDS, Oxford Ultim Max 65). The possible valence states of elements in ceramics were analyzed by X-ray photoelectron spectroscopy (XPS, K-alpha 1063, UK). The relative density (ρ_r) of each sample was determined according to the Archimedes method and was calculated by Eq. (1).

$$\rho_r = \rho_M/\rho_L \quad (1)$$

where ρ_M is the measured density and ρ_L is the theoretical density. The theoretical density ρ_L (5.676 g/cm^3) of the wurtzite ZnO lattice was calculated by the relationship of $\rho_L = (M_{Zn} + M_O)/N_A V$, where M_{Zn} is the total molar weight of Zn atoms and M_O is the total molar weight of O atoms in each mole ZnO lattice, N_A is Avogadro constant, and V is a cell volume of ZnO lattice. In order to simplify the

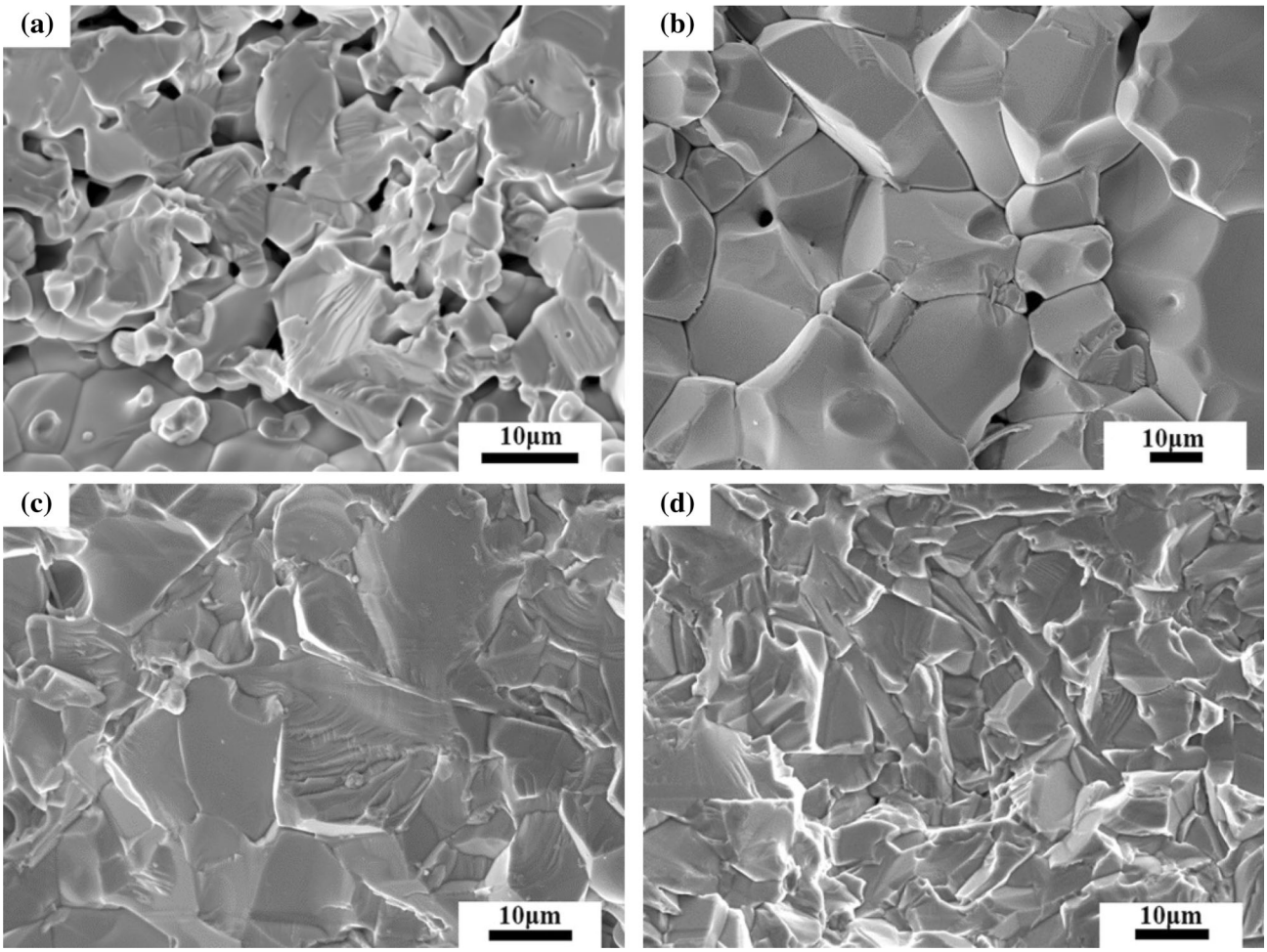

Fig. 1 SEM images of fracture surface of as-sintered ceramics, **a** ZnO without V_2O_5, **b** ZnO with 0.5% V_2O_5, **c** $Zn_{0.994}Ga_{0.006}O$ with 0.5% V_2O_5, and **d** $Zn_{0.980}Ga_{0.020}O$ with 0.5% V_2O_5

comparison of relative density of the studied ceramics, the influence of dopants and possible lattice defects in the ZnO lattice was not regarded, i.e., only the perfect ZnO lattice was taken into account for ρ_L in this work.

The temperature dependence of resistance (*R*–*T*) of each sample was measured by a resistance–temperature test system (ZWX-C, China) in temperature range from 25 to 250 °C. The resistivities were calculated according to the Ohm's law, $\rho = RA/h$, where *R* is the measured resistance, *A* is the electrode area, and *h* is the sample thickness. Two kinds of methods were used to test the electrical stability of $Zn_{1-x}Ga_xO$-based ceramics: repeated *R*–*T* measurements and measurement of the resistance change rate after aging treatment at 150 °C. Alternating current (*AC*) impedance was performed with electrochemical workstation (Gamry reference USA, 600) in frequency range from 1 Hz to 1 MHz. Each impedance spectrum was analyzed by Gamry analyst.

3 Results and discussion

3.1 Phase and microstructure

In this work, different contents of V_2O_5 (from 0.125 to 1.0% in mass ratio) were added to $Zn_{0.990}Ga_{0.010}O$ ceramics, respectively. The ρ_r of $Zn_{0.990}Ga_{0.010}O$ ceramics increased from 87.5 to 92.6% with the increase of V_2O_5 content from 0.125 to 1.0%. The increase of ρ_r becomes slow when the V_2O_5 content is more than 0.5%. So 0.5% of V_2O_5 was selected in the following experiments. The ρ_r of ZnO, $Zn_{0.994}Ga_{0.006}O$, and $Zn_{0.980}Ga_{0.020}O$ with 0.5% V_2O_5 are 90.5%, 93.2%, and 93.6%, respectively.

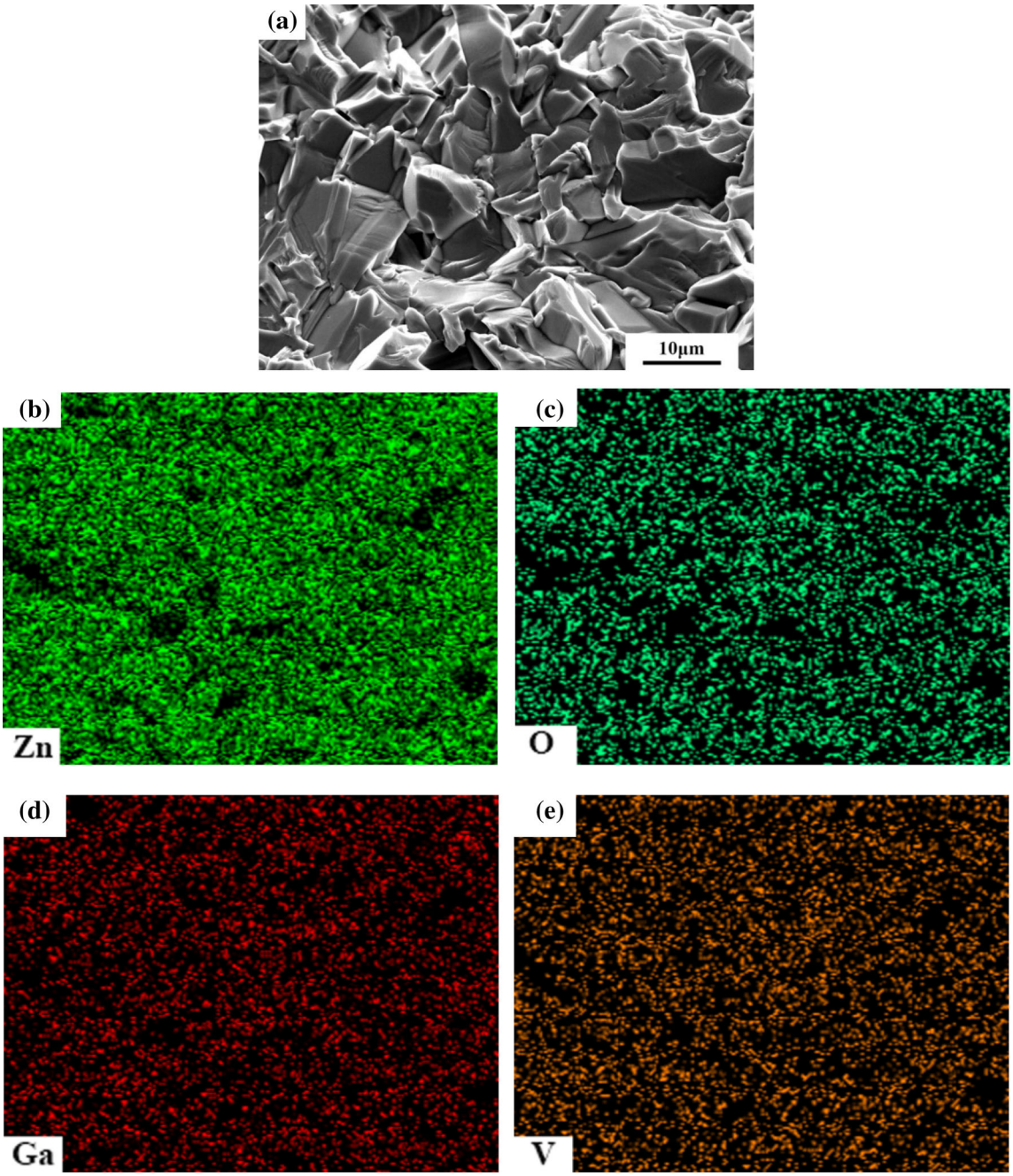

Fig. 2 SEM and elemental distribution mapping of fracture surface of $Zn_{0.990}Ga_{0.010}O$ ceramic, **a** secondary electron image in SEM, and **b–e** EDS elemental mappings of Zn, O, Ga, and V elements, respectively

Figure 1 shows SEM micrographs obtained from the fracture surfaces of as-sintered ceramics of ZnO without V_2O_5, ZnO with 0.5% V_2O_5, $Zn_{0.994}Ga_{0.006}O$ with 0.5% V_2O_5, and $Zn_{0.980}Ga_{0.020}O$ with 0.5% V_2O_5. It can be seen from Fig. 1a that the ZnO ceramic without V_2O_5 contains lots of pores. While, the pores in the ceramics with 0.5% V_2O_5 addition become much less and even vanish, as shown in Fig. 1b–d. These indicate that the addition of a small amount of V_2O_5 can effectively enhance the sintering ability of ZnO-based ceramics. This should be due to the low melting point of V_2O_5 (− 690 °C) for which the formation of liquid phase is helpful for the gas overflowing and can accelerate the mass transfer during sintering process.

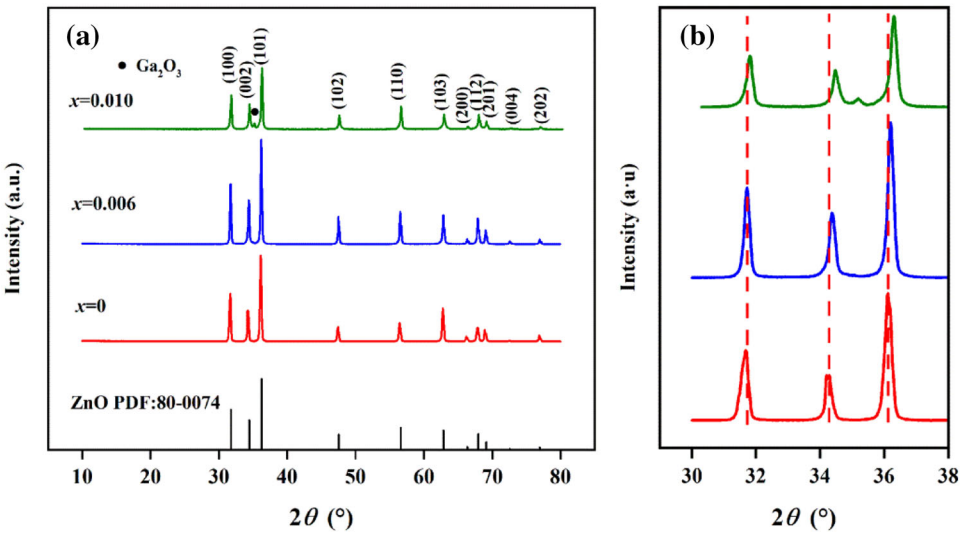

Fig. 3 XRD patterns of as-sintered $Zn_{1-x}Ga_xO$ ceramics with different contents of Ga-ions, **a** whole patterns, **b** partially enlarged view of XRD patterns

Table 1 Lattice parameters (a and c) and cell volume (V) of $Zn_{1-x}Ga_xO$ ceramics refined from the XRD patterns as shown in Fig. 1

x	a (nm)	c (nm)	V (10^{-3} nm^3)
0	0.3258	0.5212	47.91
0.006	0.3253	0.5209	47.74
0.010	0.3249	0.5203	47.58

The elemental distribution mapping of fracture surface of $Zn_{0.990}Ga_{0.010}O$ ceramic was analyzed by EDS, as shown in Fig. 2. Zn, O, Ga, and V elements are almost evenly distributed in the sample and the black area in these mappings might be caused by the roughness of the fracture surface.

Figure 3 shows XRD patterns of as-sintered $Zn_{1-x}Ga_xO$-based ceramics with 0.5% V_2O_5 (ZnO, $Zn_{0.994}Ga_{0.006}O$, and $Zn_{0.990}Ga_{0.010}O$). ZnO and $Zn_{0.994}Ga_{0.006}O$ ceramics are composed of pure hexagonal wurtzite phase with a space group of $P6_3mc$ (186) (ref. PDF No. 80–0074). While one extra diffraction peak marked by "•" as shown in Fig. 3a can be found in $Zn_{0.99}Ga_{0.010}O$ ceramic and is consistent with the diffraction of Ga_2O_3 phase (PDF Card of No. 76–0573). These imply that the solid solubility of Ga-ions in ZnO lattice might be $x < 0.010$ in this work. Figure 3b shows the magnified view of diffraction peaks with 2θ from 30° to 38°. With the increase of Ga-ion concentration, the diffraction peaks shifted toward higher diffraction angles, indicating a reduction of lattice parameters. Refined with Jade 6.0 + PDF 2004 program, the lattice parameters of hexagonal wurtzite phase for each ceramic are obtained as shown in Table 1. The reduction of lattice parameters should result from the substitution of Ga-ions in ZnO lattice for that the ionic radius of Ga^{3+} ion (0.062 nm) is smaller than that of Zn^{2+} ion (0.075 nm) [23]. At the same time, some V-cations might also substitute into the ZnO lattice, and the substitution of V-ions also reduced the ZnO-based lattice for the smaller ionic radius of V^{5+} (0.054 nm) than that of Zn^{2+} ion.

To explore the possible valence states of elements in as-sintered ceramics, $Zn_{0.990}Ga_{0.010}O$ ceramic was selected for XPS analysis and the results are shown in Fig. 4. Characteristic peaks of Zn, O, Ga, and V can be detected in the full XPS spectrum as shown in Fig. 4a. The narrow spectra for each element were fitted by Avantage 5.52 software and the results are shown in Fig. 4b–e, respectively. As shown in Fig. 4b, the peaks at binding energies of 1021.15 eV and 1044.24 eV correspond to Zn $2p_{3/2}$ and $2p_{1/2}$, respectively [24], indicating only Zn^{2+} ions exist in $Zn_{0.990}Ga_{0.010}O$ ceramic.

Figure 4c shows the narrow spectrum of O element. The spectrum of O 1 s can be fitted to be composed of two peaks. One peak locating at 531.33 eV (marked with $O_{D/A}$) should attribute to defective oxygen (O_D) and adsorbed oxygen (O_A) and the other peak at 529.89 eV corresponds to lattice oxygen (O_L) [25]. According to the areas of fitted peaks, the content ratio of $O_{D/A}$ and O_L is $[O_{D/A}]/[O_L] = 0.961$. The peaks of Ga $2p_{3/2}$ and $2p_{1/2}$ with binding energies of 1117.35 eV and 1144.12 eV, respectively, are shown in Fig. 4c, indicating that Ga-

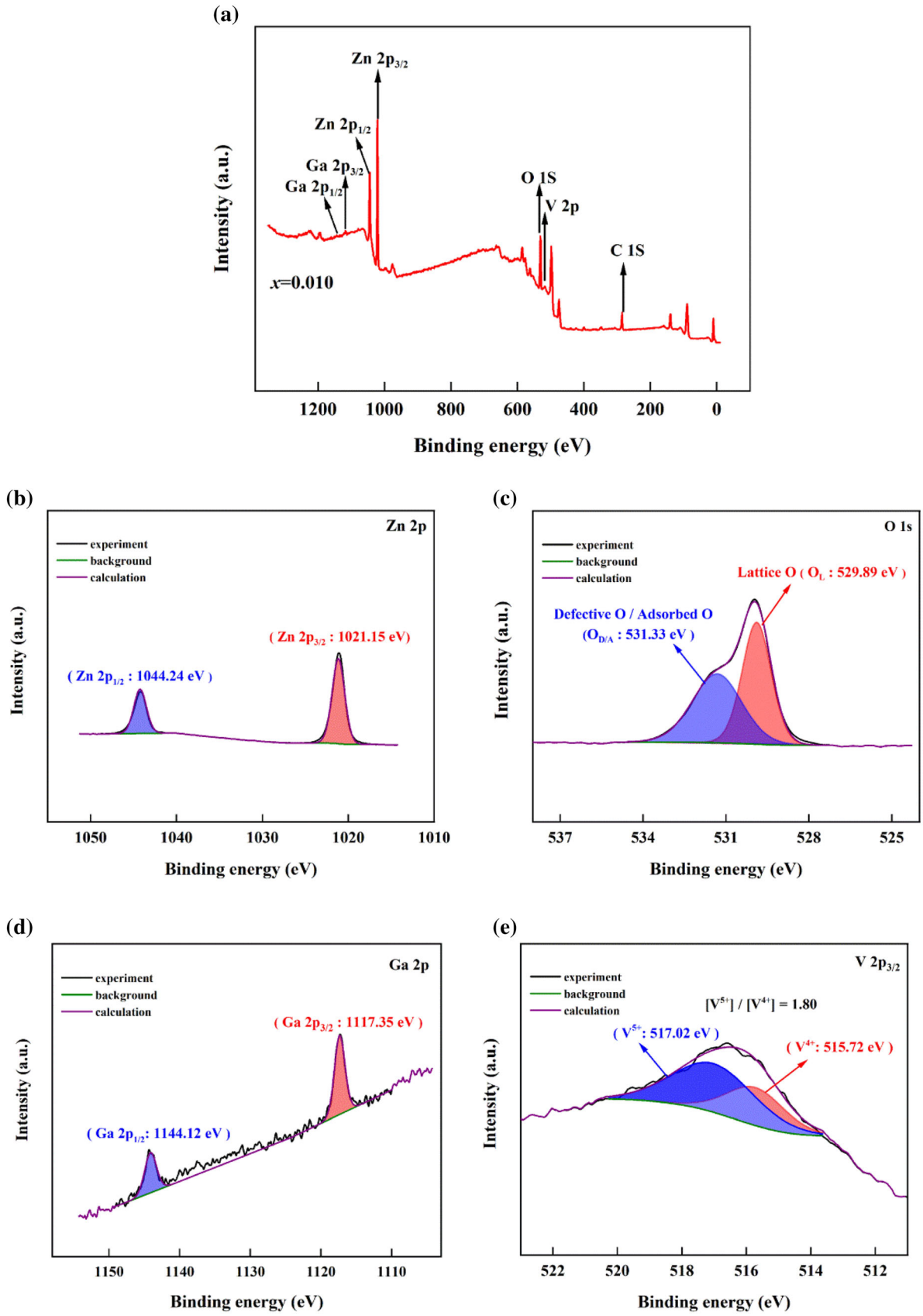
(a)
Zn 2p3/2
Zn 2p1/2
Ga 2p3/2
Ga 2p1/2
O 1S
V 2p
C 1S
x=0.010
Intensity (a.u.)
1200 1000 800 600 400 200 0
Binding energy (eV)
(b)
Zn 2p
experiment
background
calculation
(Zn 2p3/2 : 1021.15 eV)
(Zn 2p1/2 : 1044.24 eV)
Intensity (a.u.)
1050 1040 1030 1020 1010
Binding energy (eV)
(c)
O 1s
experiment
background
calculation
Lattice O (OL : 529.89 eV)
Defective O / Adsorbed O
(OD/A : 531.33 eV)
Intensity (a.u.)
537 534 531 528 525
Binding energy (eV)
(d)
Ga 2p
experiment
background
calculation
(Ga 2p3/2 : 1117.35 eV)
(Ga 2p1/2: 1144.12 eV)
Intensity (a.u.)
1150 1140 1130 1120 1110
Binding energy (eV)
(e)
V 2p3/2
experiment
background
calculation
[V5+] / [V4+] = 1.80
(V5+: 517.02 eV)
(V4+: 515.72 eV)
Intensity (a.u.)
522 520 518 516 514 512
Binding energy (eV)

◀**Fig. 4** Analysis of XPS spectra of $Zn_{0.990}Ga_{0.010}O$ ceramic, **a** XPS full spectrum, **b** Zn 2p spectrum, **c** O 1 s spectrum, **d** Ga 2p spectrum, and **e** V $2p_{3/2}$ spectrum

ion is Ga^{3+} [26]. In Fig. 4e, V $2p3_{/2}$ was detected to be composed of peaks at binding energies of 517.02 eV and 515.72 eV, respectively, indicating that V-ions in the ceramics have V^{5+} and V^{4+} valences [24]. The content ratio $[V^{5+}]$ / $[V^{4+}]$ in the ceramic is calculated to be 1.80, demonstrating that V^{5+} is the main valence state of V-ions in $Zn_{0.990}Ga_{0.010}O$ ceramic.

3.2 Electrical properties

The temperature dependence of resistivity in $\ln\rho - 1000/T$ plots of $Zn_{1-x}Ga_xO$ ceramics is shown in Fig. 5a and b. The resistivities of Ga-ion-doped ZnO ceramics decrease with the increase of temperature and display typical NTC characteristic. The nearly linear relationship of $\ln\rho - 1000/T$ follows the Arrhenius law as expressed by Eq. (2).

$$\rho_T = \rho_0 \exp\left(\frac{E_a}{kT}\right) = \rho_0 \exp\left(\frac{B}{T}\right) \quad (2)$$

where ρ_T is the resistivity at temperature T (in Kelvin), ρ_0 is a constant related to material characteristic, E_a is activation energy of conduction, k is the

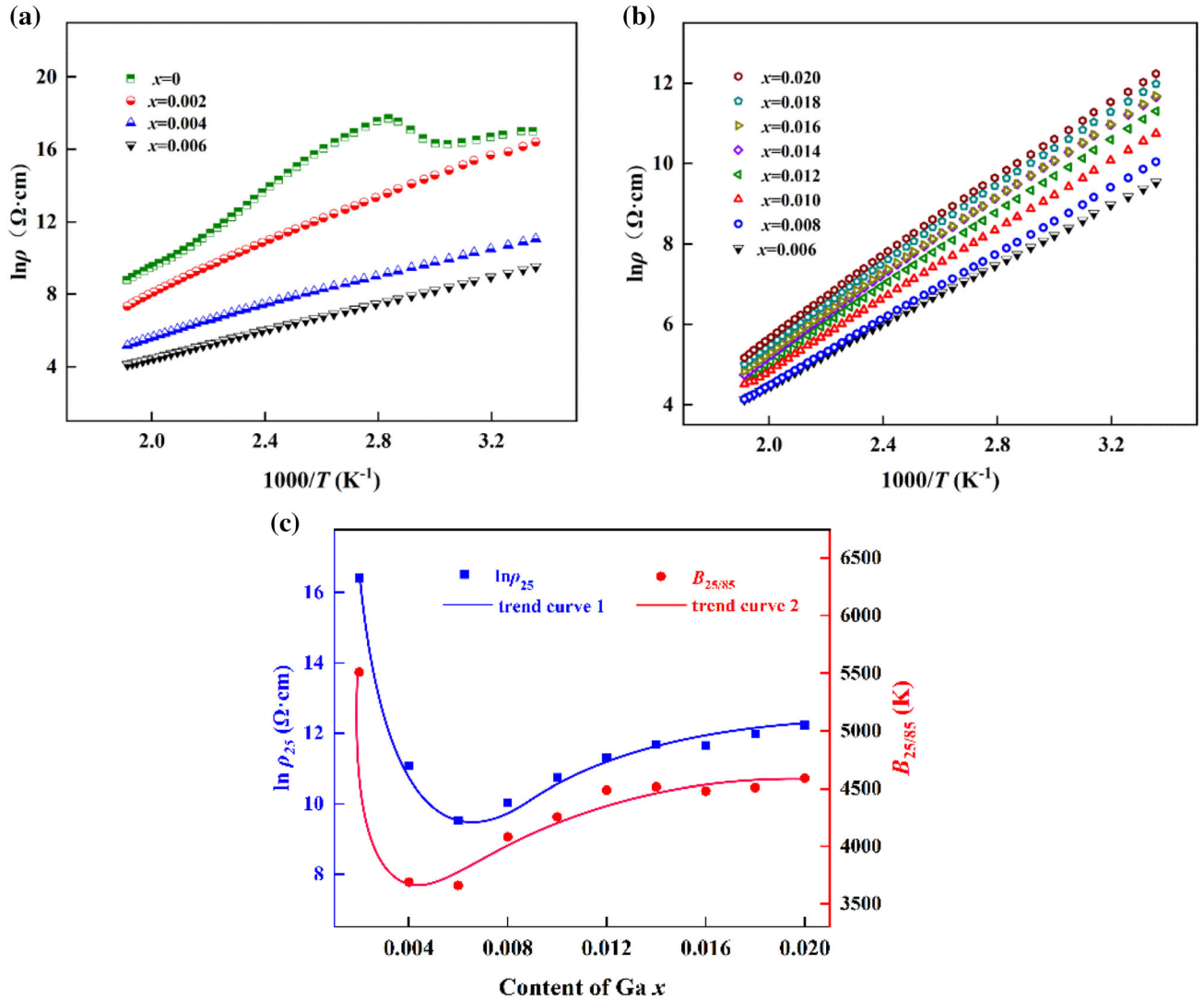

Fig. 5 Electrical properties of $Zn_{1-x}Ga_xO$ ceramics with various contents of Ga-ions **a** $0 \le x \le 0.006$, **b** $0.006 \le x \le 0.020$, and **c** Ga-ion concentration dependence of $\ln\rho_{25}$ and $B_{25/85}$

Boltzmann constant, and B is a material constant reflecting the temperature sensitivity of a NTC thermistor. The B value can be calculated by Eq. (3)

$$B = \frac{\ln \rho_1 - \ln \rho_2}{1/T_1 - 1/T_2} \tag{3}$$

where ρ_1 and ρ_2 are the resistivities at temperatures T_1 and T_2, respectively. The temperatures of T_1 and T_2 are normally selected at 298 K (25 °C) and 358 K (85 °C), respectively. So, the B value is often written as $B_{25/85}$.

Figure 5c shows the plots of Ga-content dependence of $\ln\rho_{25}$ and $B_{25/85}$ in $Zn_{1-x}Ga_xO$ ceramics. $\ln\rho_{25}$ of $Zn_{1-x}Ga_xO$ ceramics with $x \leq 0.006$ decreases with the increase of Ga-content. These should be due to the doping effect of a semiconductor. Ga^{3+} ions substituted into the ZnO lattice and introduced electron charge carriers. The related defect reaction can be expressed by Eq. (4).

$$Ga_2O_3 \xrightarrow{ZnO} 2Ga_{Zn}^{\cdot} + 2e' + 2O_O + \frac{1}{2}O_2 \tag{4}$$

Here, the weakly bound electrons at the donor level are easy to be thermally activated to the conductive band, improving the conductivity of $Zn_{1-x}Ga_xO$ ceramics. In the meanwhile, the introduced V-ions might also partially substitute into ZnO lattice, and the related defect reaction can be expressed by Eq. (5).

$$V_2O_5 \xrightarrow{ZnO} 2V_{Zn}^{\cdots} + 6e' + 2O_O + \frac{3}{2}O_2 \tag{5}$$

The substituted V-ion can act as donor and introduce electron charge carriers in the ZnO crystal. Combined with V-ions and Ga-ions, too much electrons introduced into the ZnO lattice could lead to aggregation of charge carriers, resulting in the increase of ρ_{25} when the dopant content was further increased (as shown in Fig. 5c). In the meanwhile, for the solid solubility limit of Ga-ions and V-ions in ZnO, the excessive Ga_2O_3 and V_2O_5 might segregate at the grain boundaries and enhance the grain boundary barrier, resulting in high grain boundary resistivity. On the other hand, as shown in Fig. 1, the increase of Ga-ions content in ZnO-based ceramics restrained the grain growing and increased the relative content of grain boundary accordingly. In addition, due to the large difference in porosity among ceramics, pores may have some impact on the conductivity of ceramics. So, the total resistance of ceramics increases with the increase of the content increase of Ga-ions in ZnO-based ceramics.

With the increase of Ga-ion concentration, $B_{25/85}$ values decrease first and then increase. The minimum $B_{25/85}$ value of $Zn_{0.990}Ga_{0.010}O$ ceramics is 3659 K when the content of Ga-ion (x) is 0.006. When the content of Ga-ion (x) is more than 0.006, $B_{25/85}$ values of $Zn_{1-x}Ga_xO$ ceramics are in the range of 3659–4590 K. The adjustable ρ_{25} and $B_{25/85}$ values enhance the application prospect of $Zn_{1-x}Ga_xO$ ceramics as NTC thermistors.

3.3 Impedance spectrum analysis

To understand the conduction characteristic of $Zn_{1-x}Ga_xO$ ceramics, alternating current (AC) impedance was measured and analyzed. Figure 6 shows the Nyquist plots of $Zn_{1-x}Ga_xO$ ceramics with various contents of Ga-ions measured at room temperature. The plots were fitted using equivalent circuit inset as shown in Fig. 6a. Where R_g and R_{gb} are the resistances corresponding to the grain effect and grain boundary effect, respectively, R_0 is the resistance from the measuring system, and CPE_g and CPE_{gb} are constant phase components related to internal inhomogeneity or defects. The fitted curves are in good agreement with the measured data. These reveal that the electrical properties of $Zn_{1-x}Ga_xO$ ceramics originate from both grain effect and grain boundary effect. The fitted resistance from grain effect (R_g), grain boundary one (R_{gb}), and total one ($R_t = R_g + R_{gb}$) of ceramics are shown in Table 2.

Compared with pure ZnO ceramic, both R_g and R_{gb} decreased with the increase of Ga-ions when $x < 0.006$ in $Zn_{1-x}Ga_xO$ and the decrease of R_g is greater than that of R_{gb}. These should result from the semiconductor doping effect as described in Eq. (4). Conversely, when $x > 0.006$, both R_g and R_{gb} increase with the increasing of Ga-ion concentration and the increase of R_{gb} is more than that of R_g. For solid solubility limit of Ga_2O_3 in ZnO crystal, the excessive Ga-ions may locate at the grain boundaries as impurity, such as Ga_2O_3. In the meanwhile, V_2O_5 might also locate at grain boundaries. The grain boundaries impurities hinder the electron transfer and increase the grain boundary resistance.

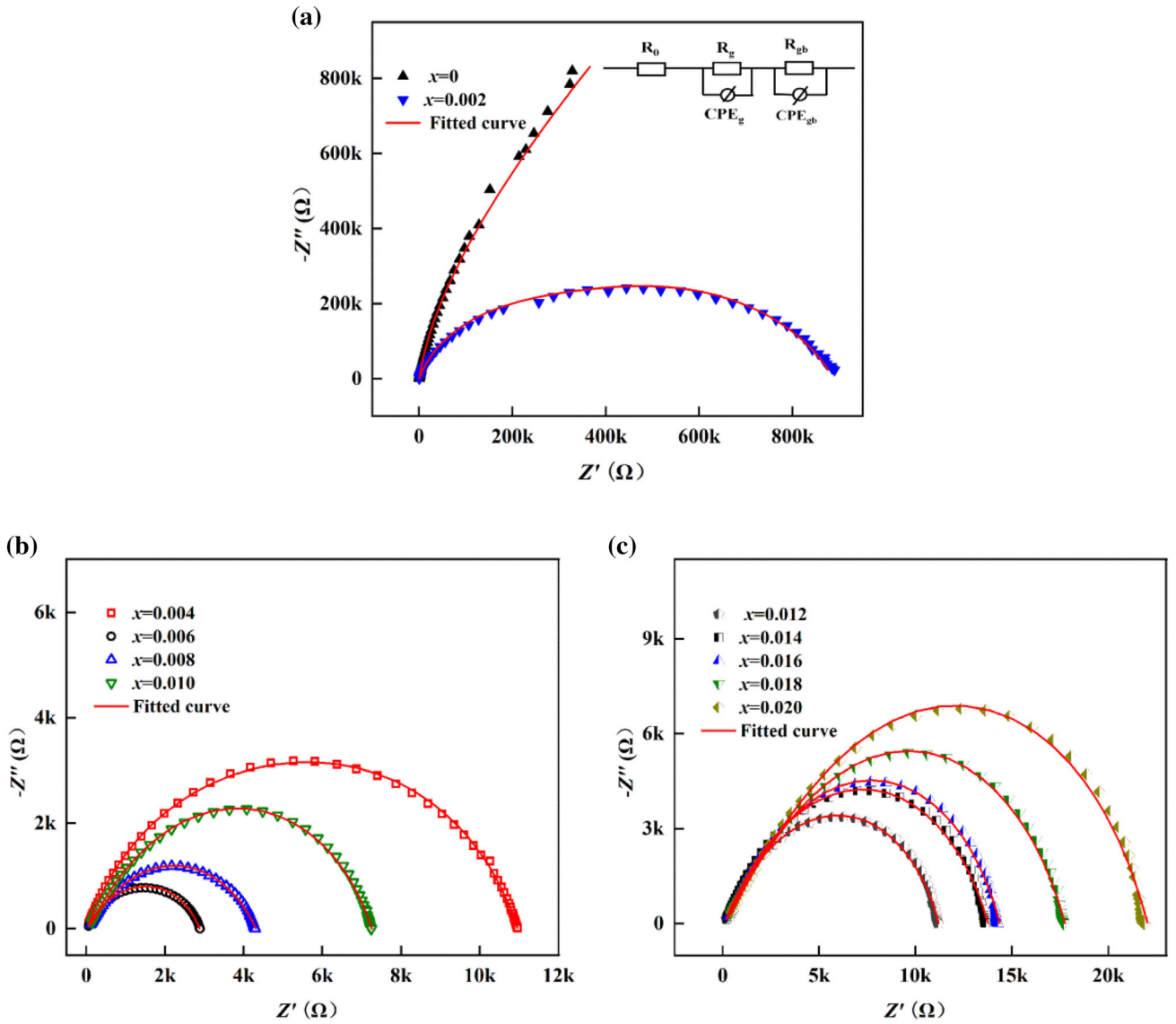

Fig. 6 Impedance spectra in Nyquist plots for $Zn_{1-x}Ga_xO$ ceramics with various contents of Ga-ions measured at room temperature, **a** x = 0, 0.002, and the inset is an equivalent circuit for plot fitting, **b** x = 0.004, 0.006, 0.008, and 0.010, and **c** x = 0.012, 0.014, 0.016, 0.018, and 0.020

Table 2 Fitted results of Nyquist plots by equivalent circuit as shown in the inset in Fig. 6a, grain resistance (R_g), grain boundary resistance (R_{gb}), total resistance ($R_t = R_g + R_{gb}$), grain capacitance (C_g), and grain boundary capacitance (C_{gb}) of $Zn_{1-x}Ga_xO$ ceramics

x	R_g (kΩ)	R_{gb} (kΩ)	R_t (kΩ)	C_g (10^{-10} F)	C_{gb} (10^{-8} F)
0	3787.1	318.7	4105.8	99.03	1.5816
0.002	656.9	230.8	887.7	70.18	2.2691
0.004	5.197	5.74	10.937	141.29	6.6693
0.006	0.385	2.469	2.854	258.18	2.9384
0.008	1.041	3.214	4.255	5.13	2.3093
0.010	1.713	5.466	7.179	127.12	1.4375
0.012	2.12	8.973	11.093	99.80	1.4276
0.014	3.3	10.35	13.65	109.29	1.1707
0.016	3.68	10.55	14.23	76.18	1.0569
0.018	5.113	12.480	17.593	48.32	0.8977
0.020	6.298	15.54	21.838	41.65	0.8337

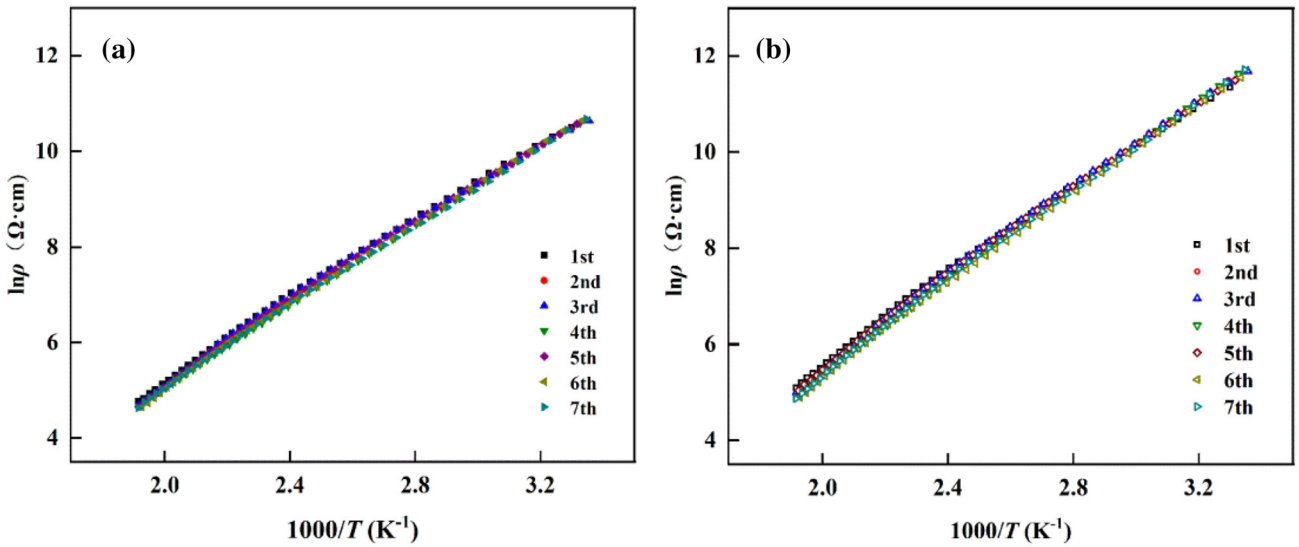

Fig. 7 Temperature dependence of resistivity ($\ln\rho$-$1/T$ plots) of $Zn_{1-x}Ga_xO$ ceramics measured repeatedly for 7 times, **a** $x = 0.010$, **b** $x = 0.020$

3.4 Electrical stability

Electrical stability is an essential property for the commercial application of NTC thermistors. Figure 7 show the plots of temperature dependence of resistivity ($\ln\rho - 1/T$ plots) tested repeatedly for seven times for $Zn_{0.990}Ga_{0.010}O$ and $Zn_{0.980}Ga_{0.020}O$ ceramics. The $\ln\rho - 1/T$ plots coincide well with each other, indicating that the $Zn_{0.990}Ga_{0.010}O$ and $Zn_{0.980}Ga_{0.020}O$ ceramics have high electrical repeatability.

$Zn_{1-x}Ga_xO$ ceramics with silver electrodes were treated at 150 °C for 1000 h to explore their electrical stability characteristics. Figure 8 shows the resistance change rate ($\Delta R/R_0$) after aging treatment for different periods. The $\Delta R/R_0$ of ZnO ceramic increased continuously during aging and is as high as 67.30% after aging for 1000 h (see in Fig. 8a). Doping with Ga-ions, the $\Delta R/R_0$ decrease obviously after aging (see in Fig. 8b, c). The $\Delta R/R_0$ of Ga-doped ceramics increase slightly in initial 600 h aging and then the resistance change rate became stable. With 1000 h of aging treatment, the final $\Delta R/R_0$ of $Zn_{1-x}Ga_xO$ is 1.41% for $x = 0.002$, 1.07% for $x = 0.004$, 1.28% for $x = 0.006$, 1.52% for $x = 0.008$, 1.49% for $x = 0.010$, 1.59% for $x = 0.012$, 1.50% for $x = 0.014$, 1.40% for $x = 0.016$, 1.68% for $x = 0.018$, and 1.85% for $x = 0.020$. These show that Ga-doped $Zn_{1-x}Ga_xO$ ceramics with V_2O_5 addition have good electrical stability.

To further explore the aging characteristics of $Zn_{1-x}Ga_xO$ ceramics, AC impedance spectra were measured for the same samples as shown in Fig. 6 after aging. The related Nyquist plots after aging were analyzed as shown in Fig. 9. The Nyquist plots were fitted with the equivalent circuit inserted in Fig. 6a. The well fitted results indicate that the electrical properties of $Zn_{1-x}Ga_xO$ ceramics after aging are still composed of grain effect and grain boundary effect. The resistance change rates of grain effect, grain boundary effect, and total effect ($\Delta R_g/R_{g0}$, $\Delta R_{gb}/R_{gb0}$, and $\Delta R_t/R_{t0}$, respectively) were calculated by comparing the related resistance before and after aging, respectively. The results are shown in Table 3. $\Delta R_t/R_{t0}$ tested by *AC* impedance method is consistent with the DC-measured results as shown in Fig. 8. Except for ZnO ceramic, R_g decreased ($\Delta R_g/R_{g0} < 0$) and R_{gb} increased ($\Delta R_{gb}/R_{gb0} > 0$) after aging. These indicate that the aging-induced increase of total resistance mainly came from the grain boundary effect.

To explore the possible origination of aging-induced evolution of electrical properties, the valence states of elements in $Zn_{0.990}Ga_{0.010}O$ ceramic after aging were investigated by XPS analysis. The XPS analysis is shown in Fig. 10. In Fig. 10a, the binding energy peaks of 1021.24 eV and 1044.32 eV correspond to Zn $2p_{3/2}$ and $2p_{1/2}$, respectively. These indicate that only Zn^{2+} ions exist in the aged

$Zn_{0.990}Ga_{0.010}O$ ceramic. The binding energies of 531.41 eV and 529.90 eV for O 1 s correspond to the peaks of the defective oxygen and/or adsorbed oxygen ($O_{D/A}$) and lattice oxygen (O_L), respectively, in the aged $Zn_{0.990}Ga_{0.010}O$ ceramic as shown in Fig. 10b. Compared with the analyzed results of the sample before aging (see in Fig. 4c), there are tiny deviations in the position of characteristic peaks for $O_{D/A}$ and O_L after aging. The ratio of $[O_{D/A}]/[O_L]$ after aging is 1.58 and is quite different from that before aging (0.961).

The peaks of the $2p_{3/2}$ and $2p_{1/2}$ orbital energy spectra of Ga are shown in Fig. 10c. The peaks of binding energies of 1117.48 eV and 1144.25 eV indicate that Ga-element has the valence of Ga^{3+} in the aged $Zn_{0.990}Ga_{0.010}O$ ceramic. The XPS spectrum of V-cations in $Zn_{0.990}Ga_{0.010}O$ ceramic after aging is shown in Fig. 10d. The analysis shows that the XPS spectrum is composed of peaks with binding energies of 517.01 eV and 515.61 eV, respectively. It indicates that V-ions have V^{5+} and V^{4+} kind of valences in the aged $Zn_{0.990}Ga_{0.010}O$ ceramic. The $[V^{5+}]/[V^{4+}]$ ratio in the aged ceramic is 2.92, which is higher than that in the sample before aging ($[V^{5+}]/[V^{4+}] = 1.80$ as analyzed in Fig. 4e).

According to the analysis of O- and V-XPS spectra as discussed in Figs. 4c and e and 10b and d, both the $[O_{D/A}]/[O_L]$ and $[V^{5+}]/[V^{4+}]$ increased after aging treatment. These imply that the aging process should be closely related to oxygen adsorption and the

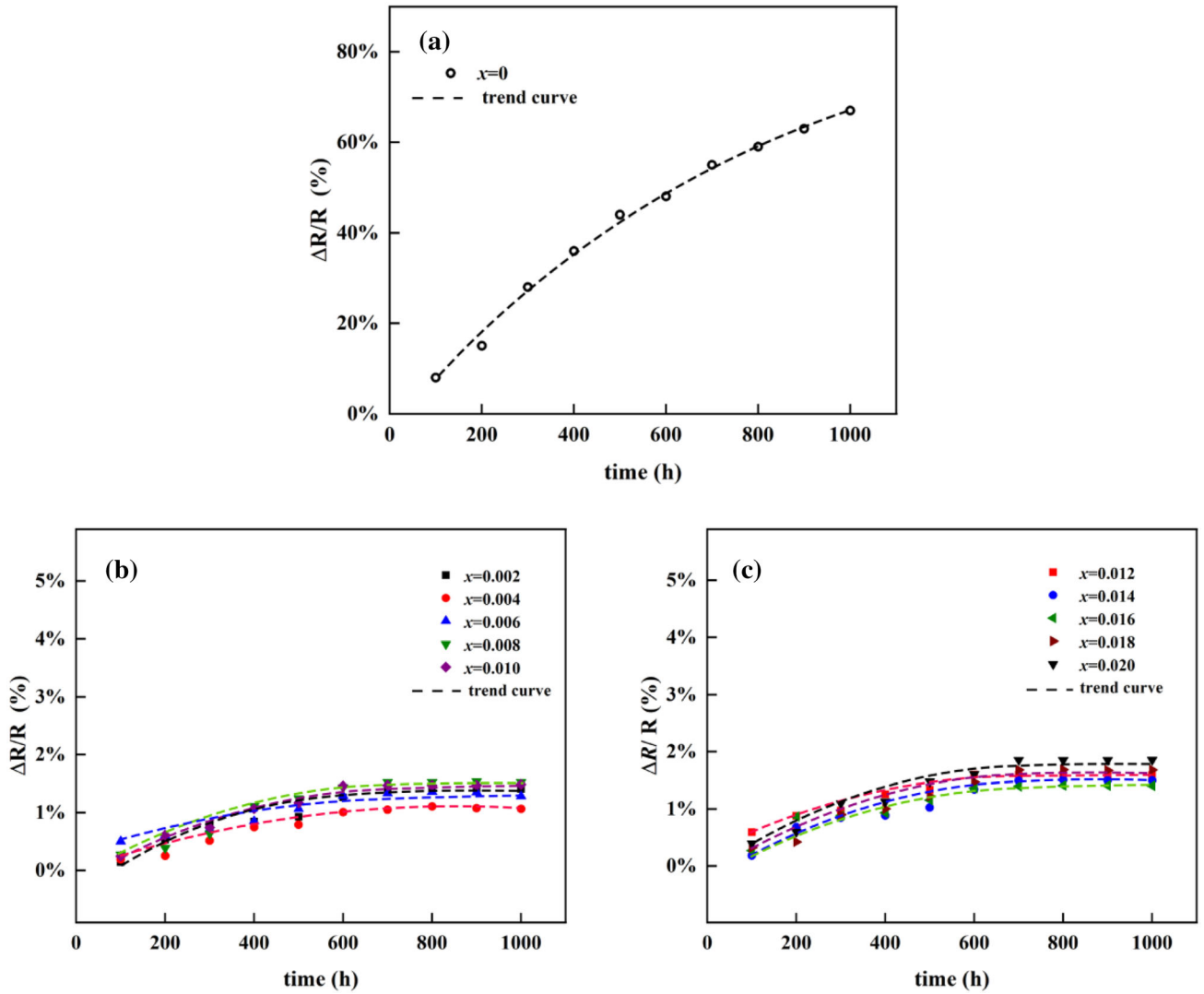

Fig. 8 Resistance change rate ($\Delta R/R_0$) of $Zn_{1-x}Ga_xO$ ceramics with V_2O_5 as sintering aids aged at 150 °C for different periods, **a** $x = 0$, **b** $x = 0.002$, 0.004, 0.006, 0.008, and 0.010, and **c** $x = 0.012$, 0.014, 0.016, 0.018, and 0.020

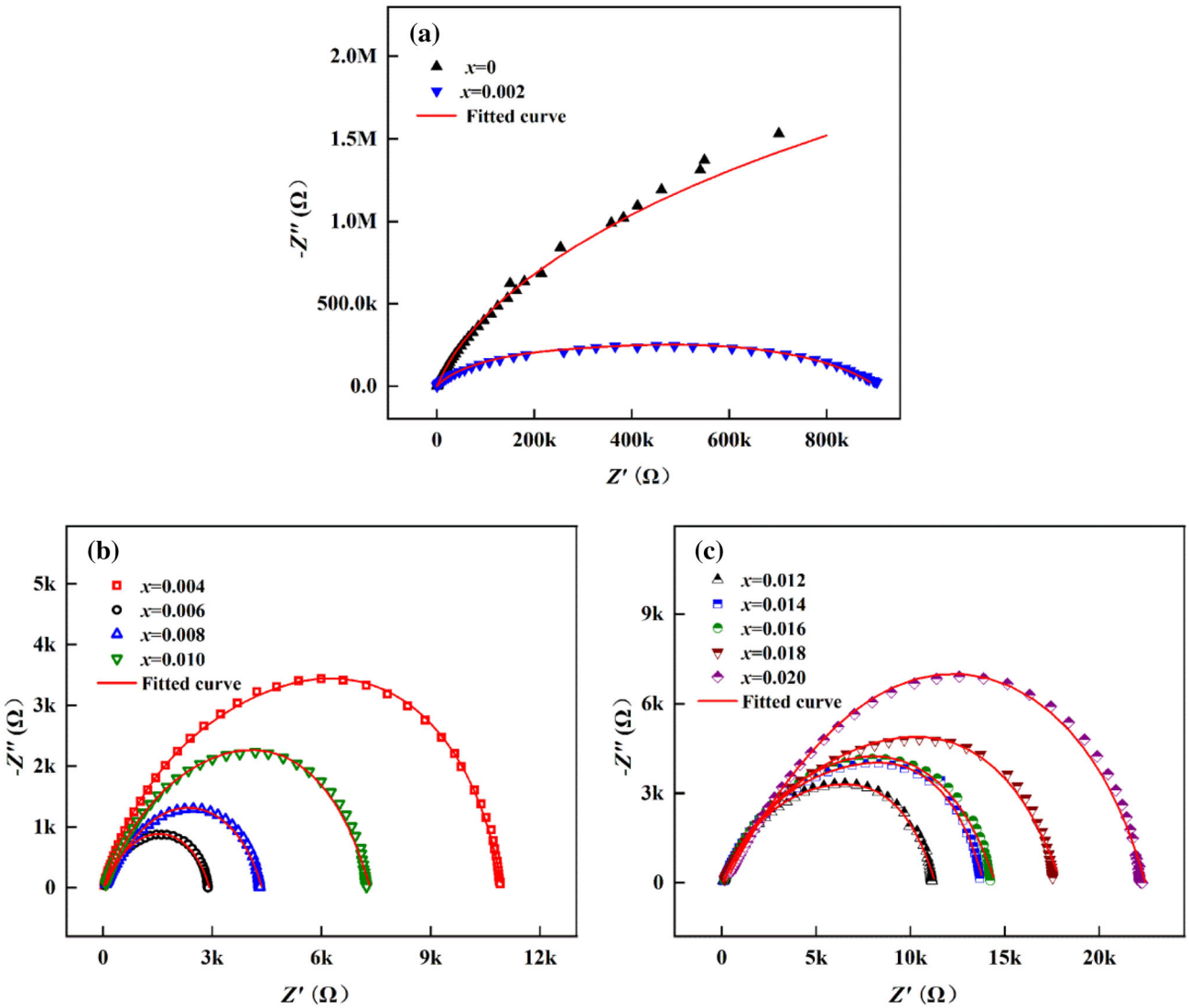

Fig. 9 Impedance spectra in Nyquist plots of $Zn_{1-x}Ga_xO$ ceramics aged for 1000 h, **a** x = 0 and x = 0.002, **b** x = 0.004, 0.006, 0.008, and 0.010, and **c** x = 0.012, 0.014, 0.016, 0.018, and 0.020

Table 3 R_g, R_{gb}, R_t, $\Delta R_g/R_{g0}$, $\Delta R_{gb}/R_{gb0}$, and $\Delta R_t/R_{t0}$of $Zn_{1-x}Ga_xO$ ceramics aged for 1000 h

x	R_g (kΩ)	R_{gb} (kΩ)	R_t (kΩ)	$\Delta R_g/R_{g0}$ (%)	$\Delta R_{gb}/R_{gb0}$ (%)	$\Delta R_t/R_{t0}$ (%)
0	1862	5239.90	7101.90	16.98	97.51	67.30
0.002	226.90	673.41	900.31	-1.69	2.51	1.42
0.004	5.10	5.95	11.05	-1.85	3.71	1.07
0.006	0.375	2.516	2.89	-2.80	1.90	1.30
0.008	1.02	3.30	4.32	-1.99	2.66	1.52
0.010	1.702	5.585	7.287	-0.65	2.17	1.50
0.012	2.10	9.17	11.27	-0.87	2.17	1.59
0.014	3.28	10.58	13.86	-0.67	2.20	1.51
0.016	3.67	10.76	14.43	-0.20	1.96	1.40
0.018	5.11	12.81	17.92	-0.19	2.46	1.69
0.020	6.26	15.98	22.24	-0.57	2.80	1.83

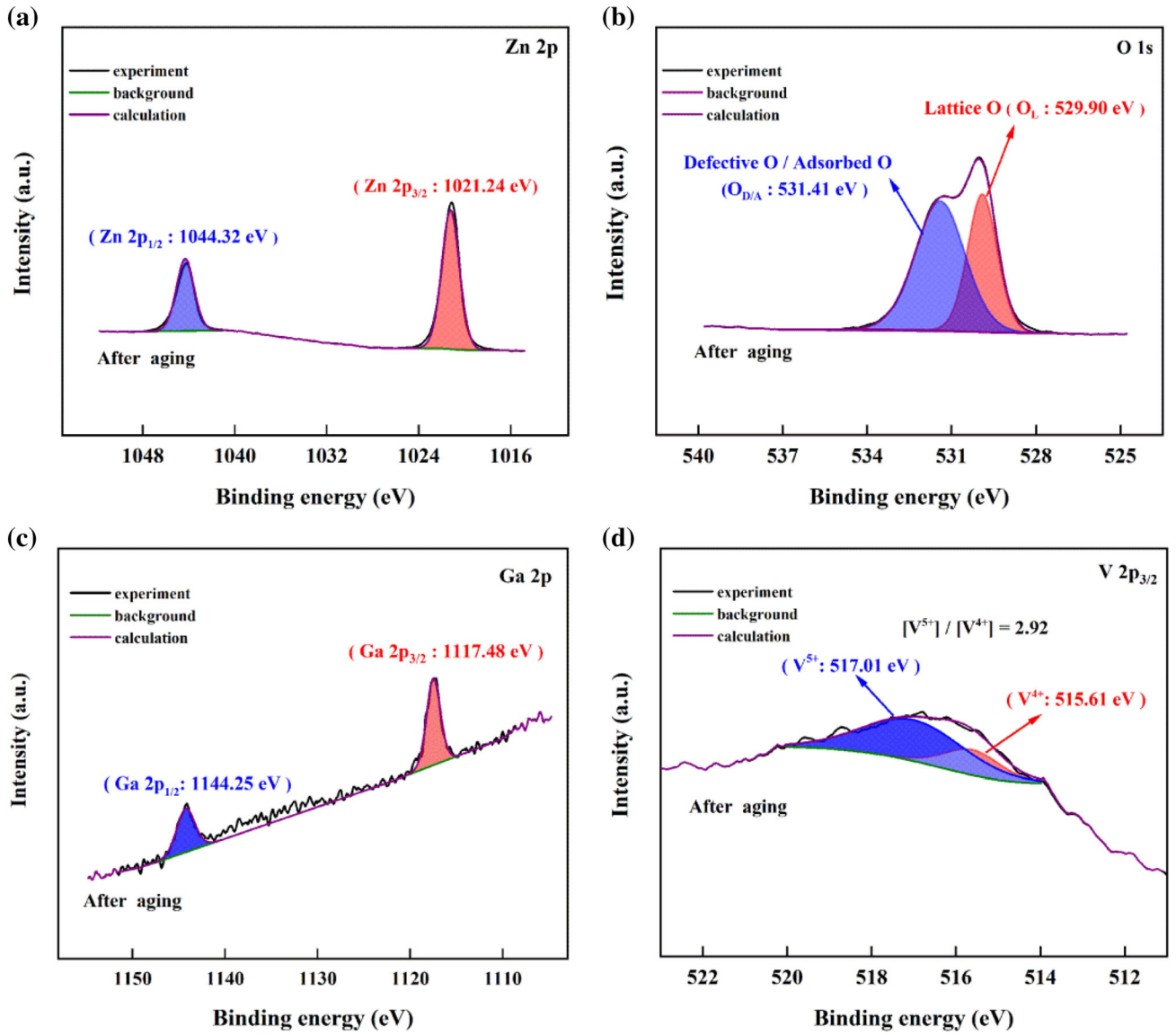

Fig. 10 XPS spectra of $Zn_{0.990}Ga_{0.010}O$ ceramic after aging, **a** Zn 2p, **b** O 1 s, **c** Ga 2p, and **d** V $2p_{3/2}$

change of V-ionic valence. Oxygen molecules (O_2) in the aging environment might adhere on the ceramic surface. The adhered O_2 may capture electrons from the ceramic body and turns into the adsorbed oxygen (O_{2ad}) and even undergoes the procedure of $O_{2ad} \rightarrow O^-_{2ad}\cdot \rightarrow O^-_{ad} \rightarrow O^{2-}$ [27, 28]. So, the reactive species of $O^-_{2ad}\cdot$ and oxygen ions (O^{2-}) are formed. This procedure resulted in the increase of $O_{D/A}$ quantity and $[O_{D/A}]/[O_L]$ ratio. At the same time, the variation of oxygen species must capture electrons from the ceramic body (both grains and grain boundaries). As in the analysis of XPS spectra, the valence state of V-ions changed during aging. So the captured electrons by $O_{D/A}$ should mainly come from V-ions, i.e., partial V^{4+} ions were oxidized to V^{5+} ions, resulting in the higher $[V^{5+}]/[V^{4+}]$ ratio in the aged ceramic.

There might be two sources for the captured electrons by $O_{D/A}$, directly from grain boundaries or from intragranular crystals. When the electrons were captured from the intragranular crystals, the segregation degree of excessive charge carriers induced by excessive doping Ga- and V- ions reduced, as discussed in Fig. 5c, resulting in the slight decrease of resistivity of the grain effect. These are in agreement with the results as analyzed in Fig. 9 and Table 3. When the $O_{D/A}$-captured electrons come from the grain boundaries, the electron should originate from the V-ions for that vanadium oxides as sintering aids

might locate at the grain boundaries. The defect reaction of $V^{4+} - e' \rightarrow V^{5+}$ took place and increased the $[V^{5+}]/[V^{4+}]$ ratio. This process enhanced the Schottky barrier at grain boundaries and increased the resistivity of the grain boundary effect.

4 Conclusion

0.5% (mass ratio) of V_2O_5 can enhance the sintering ability of Ga-doped ZnO ($Zn_{1-x}Ga_xO$) ceramics. V_2O_5-modified $Zn_{1-x}Ga_xO$ exhibits typical NTC characteristics and has high temperature sensitivity with material constant of $B_{25/85}$ from 3659 to 4590 K. The prepared ZnO-based NTC ceramics show high electrical stability with resistance change rate ($\Delta R/R_0$) less than 1.85% after aged at 150 °C for 1000 h. The aging-induced resistance change rate is mainly due to the increase of grain boundary resistance. The aging process is proposed to include the following factors: the adsorbed oxygen captures electrons from the ceramics, the quantity of defect oxygen, and $[V^{5+}]/[V^{4+}]$ ratio increases in the ZnO-based NTC ceramics.

Acknowledgements

This work is supported by the research funds from the National Natural Science Foundation of China (No. 51767021), Research and development program in key areas of Guangdong Province, China (No. 2019B090913002), and the General Project of Scientific Research Project of Hunan Provincial Department of Education Scientific, China (No. 19C0342).

Declarations

Conflict of interest The authors declare that they do not have any financial interest or personal relationship with any other people or organization that could inappropriately influence (bias) the present work.

References

1. K. Park, Microstructure and electrical properties of $Ni_{1.0}Mn_{2-x}Zr_{xO4}$ ($0 \le x \le 1.0$) negative temperature coefficient thermistors. Mater. Sci. Eng. B **104**, 9–14 (2003)
2. C. Ma, H. Gao, TEM and electrical properties characterizations of $Co_{0.98}Mn_{2.02}O_4$ NTC ceramic. J. Alloys Compd. **749**, 853–858 (2018)
3. W. Hao, H. Zhang, C. Gao, B. Li, Z. Ma, Z. Li, Influence of V/Ni-doping on electrical properties and aging stability of $ZnFe_2O_4$-based NTC ceramics. J. Mater. Sci. Mater. Electron. **32**, 17800–17809 (2021)
4. M. Chen, H. Zhang, T. Liu, H. Jiang, A. Chang, Preparation, structure and electrical properties of $La_{1-x}Ba_xCrO_3$ NTC ceramics. J. Mater. Sci. Mater. Electron. **28**, 18873–18878 (2017)
5. J. Wang, H. Zhang, D. Xue, Z. Li, Electrical properties of hexagonal $BaTi_{0.8}Co_{0.2}O_{3-\delta}$ ceramic with NTC effect. J. Phys. D **42**, 235103 (2009)
6. F. Guan, Z. Dang, S. Huang, J. Wang, I. Milisavljevic, D. Carloni, X. Cheng, Y. Wu, LaCr1-xFexO3 ($0 \le x \le 0.7$): A novel NTC ceramic with high stability. J. Eur. Ceram. Soc. **40**, 5597–5601 (2020)
7. G. Jiang, Z. Li, C. You, W. Hao, Z. Ma, H. Zhang, Temperature sensitivity and electrical stability of Sb/Mn co-doped SnO_2 ceramics. J. Mater. Sci. Mater. Electron. **32**, 16945–16955 (2021)
8. X. Wang, Z. Li, W. Yan, P. Wang, H. Zhang, Electrical properties of Nb/Al-doped CuO-based ceramics for NTC thermistors. Process. Appl. Ceram. **14**, 47–55 (2020)
9. Z. Guo, J. Shao, H. Lin, M. Jiang, S. Chen, Z. Li, Electrical conductivity & temperature sensitivity of ceramics based on NiO simple oxides for NTC applications. J. Mater. Sci. Mater. Electron. **28**, 11871–11877 (2017)
10. Q. Wang, W. Kong, J. Yao, A. Chang, Fabrication and electrical properties of the fast response $Mn_{1.2}Co_{1.5}Ni_{0.3}O_4$ miniature NTC chip thermistors. Ceram. Int. **45**, 378–383 (2019)
11. J. Wang, J. Zhang, Structural and electrical properties of $NiMg_xMn_{2-x}O_4$ NTC thermistors prepared by using sol–gel derived powders. Mater. Sci. Eng. B **176**, 616–619 (2011)
12. Z. Yang, H. Zhang, Z. He, B. Li, Z. Li, Influence of B^{3+}- and Na^+-ions on electrical property and temperature sensitivity of NiO-based ceramics. J. Mater. Sci. Mater. Electron. **30**, 3088–3097 (2019)
13. J. Wang, H. Zhang, X. Sun, Y. Liu, Z. Li, Electrical properties and temperature sensitivity of Li/Fe-modified NiO-based ceramics as NTC thermistors. J. Mater. Sci. Mater. Electron. **27**, 11902–11908 (2016)
14. B. Yang, H. Zhang, J. Zhang, X. Zhang, Z. Li, Electrical properties and temperature sensitivity of B-substituted CuO-based ceramics for negative temperature coefficient thermistors. J. Mater. Sci. Mater. Electron. **26**, 10151–10158 (2015)
15. H. Li, I.P.L. Thayil, X. Ma, X. Sang, H. Zhang, A. Chang, Electrical properties and aging behavior of Na-doped

$Mn_{1.95}Co_{0.21}Ni_{0.84}O_4$ NTC ceramics. Ceram. Int. **46**, 24365–24370 (2020)
16. C. Gao, Z. Li, L. Yang, D. Peng, H. Zhang, Investigation of electrical and aging properties of Bi-modified $(Zn_{0.4}Ni_{0.6})_{1-x}Na_xO$ ceramic thermistors. J. Eur. Ceram. Soc. **41**, 4160–4166 (2021)
17. H. Zeng, G. Duan, Y. Li, S. Yang, X. Xu, W. Cai, Blue luminescence of ZnO nanoparticles based on non-equilibrium processes: defect origins and emission controls. Adv. Funct. Mater. **20**, 561–572 (2010)
18. Y. Zhu, L. Zhou, Q. Jiang, One-dimensional ZnO nanowires grown on three-dimensional scaffolds for improved photocatalytic activity. Ceram. Int. **46**, 1158–1163 (2020)
19. M. Ha, S. Lim, J. Park, D.S. Um, Y. Lee, H. Ko, Bioinspired interlocked and hierarchical design of ZnO nanowire arrays for static and dynamic pressure-sensitive electronic skins. Adv. Funct. Mater. **25**, 2841–2849 (2015)
20. Z.L. Wang, J. Song, Piezoelectric nanogenerators based on zinc oxide nanowire arrays. Science **312**, 242–246 (2006)
21. S. Li, H. Zhang, S. Leng, Z. Yang, J. Shao, Z. Li, Characterization of temperature induced resistivity jump in Li/Y/Cr co-doped ZnO ceramics. J. Mater. Sci. Mater. Electron. **29**, 10969–10975 (2018)
22. P. Li, H. Zhang, C. Gao, G. Jiang, Z. Li, Electrical property of Al/La/Cu modified ZnO-based negative temperature coefficient (NTC) ceramics with high ageing stability. J. Mater. Sci. Mater. Electron. **30**, 9598–19608 (2019)
23. J. Fan, S. Leng, Z. Cao, W. He, Y. Gao, J. Liu, G. Li, Colossal permittivity of Sb and Ga co-doped rutile TiO_2 ceramics. Ceram. Int. **45**, 1001–1010 (2019)
24. M.C. Biesinger, L.W.M. Lau, A.R. Gerson, R.S.C. Smart, Resolving surface chemical states in XPS analysis of first row transition metals, oxides and hydroxides: Sc, Ti, V, Cu, and Zn. Appl. Surf. Sci. **257**, 887–898 (2010)
25. Y. Niu, X. Yin, C. Sun, X. Song, N. Zhang, Adjusting surface oxygen vacancies prompted perovskite as high performance cathode for solid oxide fuel cell. J. Alloys Compd. **865**, 158746 (2021)
26. R.J. Iwanowskia, M.H. Heinonenb, I. Prackac, J. Kachniarza, XPS characterization of single crystalline $SrLaGa_3O_7$:Nd. Appl. Surf. Sci. **283**, 168–174 (2013)
27. J. Chen, Z. Chen, X. Zhang, X. Li, L. Yu, D. Li, Antimony oxide hydrate ($Sb_2O_5{\cdot}3H_2O$) as a simple and high efficient photocatalyst for oxidation of benzene. Appl. Catal. B **210**, 379–385 (2017)
28. G. Zou, Y. Xu, S. Wang, M. Chen, W. Shangguan, The synergistic effect in Co-Ce oxides for catalytic oxidation of diesel soot. Catal. Sci. Technol. **5**, 1084–1092 (2015)